Measurement of temperature and vapour distribution in an evaporating DISI-spray under engine relevant conditions using two-line excitation laser-induced fluorescence

Johannes Trost, Lars Zigan*, Alfred Leipertz
Dept. Engineering Thermodynamics (LTT) and Erlangen Graduate School in Advanced Optical Technologies (SAOT), FAU Erlangen-Nuremberg, Germany
Johannes.Trost@ltt.uni-erlangen.de and Lars.Zigan@cbi.uni-erlangen.de

Abstract

The main objective in the development of modern IC-engines is the reduction of fuel consumption and pollutant emission. Direct-Injection Spark-Ignition (DISI) strategies are commonly used and especially spray-guided concepts (SG-DISI) offer a high potential to reduce fuel consumption. However, the mixture is not homogeneous through the combustion chamber, and therefore, local hot spots or low temperature regions can appear. Planar laser-induced fluorescence (PLIF) with two-line excitation is an approved method to measure temperature and fuel vapor distribution under engine relevant conditions. In this study this technique is optimized for simultaneous mass fraction and temperature measurements in DISI sprays. The non-fluorescent surrogate fuel iso-octane with the fluorescence tracer 3-pentanone is used to analyse the jet of a multi-hole injector. The tracer is calibrated with high accuracy using a high temperature calibration cell. Averaged results of the spray measurement are compared to a CFD-simulation, which shows in general a good agreement. Single-shot results are used to analyse cyclic fluctuations of the spray. A detailed error analysis validates the capability of this technique as inaccuracy for the temperature of 3.8% and for the mass fraction of 5.5% were achieved for ensemble averaged measurements, which are useful for model improvements.

Introduction

The main objective in the development of modern IC engines is the reduction of pollutant emission and fuel consumption. Direct-injection spark-ignition (DISI) engine concepts are already widely used in the automotive industry and provide a promising capability of further improvement. With spray guided mixture formation controlled fuel stratification for partial load conditions can be achieved, reducing the fuel consumption. Another advantage in efficiency of direct injection is the evaporation cooling of the fuel, which allows a higher compression. The fuel injection reduces the cylinder temperature, so that engine knock can be avoided despite higher compression ratios. The mixture formation is not homogeneous throughout the cylinder, so temperature cannot be calculated by thermodynamic analysis assuming a homogenous charge. Due to these inhomogeneities, highly charged DISI engines may tend to unwanted auto-ignition or pre-ignition [1]. Moreover, mixture formation and ignitability for fuel stratification conditions for late injection timing are determined by inhomogeneous temperature fields throughout the cylinder and the spray, which leads to different local evaporation rates. Hence, a spatial and temporal resolved measurement of the temperature and fuel concentration during injection is required to locally resolve evaporation rate and cooling in the spray.

Up to now, there are very few measurements to determine the temperature and vapor concentration fields in sprays with optical techniques at engine conditions. Planar laser-induced fluorescence (PLIF) of fuel tracers is the most promising method to simultaneously determine temperature and fuel distribution in the gas phase. Typical tracers such as acetone [2, 3], 3-pentanone [4, 5], toluene [6-8], naphthalene [9, 10] and recently fluoranthene [11] are used. The highest accuracy and precision are obtained with two-line excitation of ketones. Löffler et al. [3] reported a precision of 2-3% for two-line excitation of acetone in a flow cell at homogeneous temperature distribution (573 K), whereas Luong et al. [7] realized a single-shot precision of 5.5% at 600 K for toluene with homogeneous charge in a motored engine. For the examination of iso-octane, a suitable tracer is 3-pentanone [4, 5], due to its similar physical properties such as molecular mass, normal boiling point, liquid kinematic viscosity and heat of evaporation. Rothamer et al. [5] showed a maximum achievable precision of 2.1% at 600 K with two excitation wavelengths at 277 nm / 308 nm of 3-pentanone in a motored engine and a measurement inaccuracy of 4%.

Moreover, tracing the fuel with LIF-dopants introduces some complexities that may change the injection and spray processes leading to significant systematic errors that make a quantification of the gas phase difficult. The fuel-tracer mixture may show a changed atomization, especially the fuel viscosity significantly changes the internal nozzle flow and the atomization behavior [12]. However, the viscosity differences in the iso-octane/3-

* Corresponding author: lars.zigan@cbi.uni-erlangen.de

pentanone mixture applied in this study are relatively small and can therefore be neglected. Moreover, the evaporation of multi-component fuels (such as fuel-tracer mixtures) can show demixing of fuel components in the droplet under DISI conditions with injection in high-pressure atmosphere [12-16]. It was also reported that mixtures of 3-pentanone and iso-octane behave in a non-ideal manner [17] even though the normal boiling points of the components are well matched. However, the mixing process inside a droplet in a turbulent flow may show different results and lead to varied conclusions as reviewed by Schulz and Sick [18]. Another problem is tracer decomposition occurring at high temperatures and long residence time of the tracer [19] in hot atmosphere during fluorescence-calibration or reference measurements with homogeneous tracer distribution, which can lead to inaccuracies in quantification of concentration or temperature for low signal-to-noise ratios.

The present paper shows the results of a simultaneous spatial resolved measurement of mass fraction and temperature of an evaporating iso-octane spray under DISI-engine conditions with two-line excitation LIF based on 3-pentanone. The measurements are compared to results of a Computational Fluid Dynamics (CFD) spray model to show the capability of the measurement technique. Additionally, a precise tracer calibration under relevant conditions is presented.

Measurement principle

Laser-induced fluorescence with ketones as tracer is a commonly used measurement technique for IC engine applications [2-5]. The major advantages of this technique are the strong intensity and red shift of its signal that enables low-noise detection even at short exposure times and a separation of the exciting laser light by means of an optical filter. Furthermore, its high temporal and spatial resolution is ideal for imaging in an engine spray. In general, the fluorescence signal intensity S_{fl} can be calculated by

$$S_{fl}=\eta \cdot E \cdot \rho_{tracer} \cdot \sigma(\lambda,T) \cdot \phi(\lambda,T,p,\chi_i) \tag{1}$$

where η is the optical efficiency factor of the setup, E is the laser pulse energy, ρ_{tracer} is the tracer density, $\sigma(\lambda,T)$ is the absorption cross section as a function of the temperature T and excitation wavelength λ and $\phi(\lambda,T,p,\chi_i)$ is the fluorescence quantum yield as a function of temperature T, pressure p, wavelength λ and bath gas composition χ_i. The optical efficiency factor η can be eliminated by normalizing the signal to a reference signal of known temperature, pressure and bath gas composition and identical optical parameters. Normalized signals and laser energies will be written with a "norm" in the subscript here forth. The laser pulse energy E can be measured with an energy meter. The pressure can usually be assumed to be a global quantity and, therefore, taken from a pressure transducer.

The tracer can be excited with two different laser sources (denoted in the subscript by *L1* and *L2*, respectively) with a small temporal separation, during which the temperature and concentration fields do not change (typically few microseconds). Then, two quasi-simultaneous signals of the same state can be acquired (two-line excitation). By building the ratio S_R of the normalized signals, the influence of the tracer density cancels out.

$$S_R = \frac{S_{L1,\,norm}}{S_{L2,\,norm}} = \frac{E_{L1,norm} \cdot \sigma(\lambda_{L1},T) \cdot \phi(\lambda_{L1},T,p,\chi_i)}{E_{L2,norm} \cdot \sigma(\lambda_{L2},T) \cdot \phi(\lambda_{L2},T,p,\chi_i)} \tag{2}$$

The measurements in the present study were performed with iso-octane in nitrogen atmosphere to prevent ignition. Iso-octane is assumed to have no influence on the fluorescence behavior of the tracer and the bath gas is pure nitrogen. With the known bath gas composition, the only remaining unknown factor is the temperature T that can then be calculated from

$$T = f(S_R, p). \tag{3}$$

The tracer density can then be calculated with the obtained temperature from one of the two signals.

$$\rho_{tracer} = f(S_{L1,\,norm}, T, p) \tag{4}$$

The dependency of the signal intensity of the tracer on temperature, pressure and bath gas composition has to be known for this measurement technique. Therefore, the tracer 3-pentanone was calibrated in nitrogen atmosphere under the investigated spray conditions using a flow cell.

Experimental setup

The following section describes the experimental setup used for the tracer calibration and the spray measurement. The tracer 3-pentanone is calibrated using a high temperature calibration cell (HTC^2). A constant nitro-

gen flow regulated by a high precision mass flow controller is heated and passed through the cell. The evaporated tracer is added after the heater to avoid contact with the hot surface of the heater. The amount of tracer is also regulated by a high precision mass flow controller. After a short mixing section the homogeneous mixture passes the main body of the cell, which is equipped with four fused silica windows for optical access in the UV. The temperature inside the cell is measured with two thermocouples in the centre of the stream directly above and below the windows. The pressure is taken from a pressure transducer that is connected to the cell with a pipe of 1 mm inner diameter and about 50 mm length to avoid heating of the sensor. The spray measurements are conducted in an optically accessible combustion test rig ("OptiVeP") that is designed for spray investigations at conditions up to 10 MPa and 1000 K [20]. A constant nitrogen flow can be set up with high precision mass flow controllers and pumped through the test rig, so that the whole volume (about 7 l) can be flushed completely within 2 s to remove fuel between injections. For the present study the chamber pressure and temperature are set to 0.8 MPa and 673 K, respectively, to model late injection timing. A 6-hole solenoid injector is mounted at the bottom of the test rig. As surrogate fuel iso-octane with 20% 3-pentanone (by volume) as fluorescence tracer is used. The fuel and the injector are conditioned to 353 K similar to engine wall temperatures. The injection pressure is set to 10 MPa and the injection duration is 1,000 µs, which results in an injected mass of 12.4 mg/pulse. The geometric spray angle of the nozzle is 55°, the bent angle is 10°.

Except the camera, the optical setup is the same for calibration and spray measurement, even identical components are used. Figure 1 shows a sketch of the setup. For the excitation, a KrF excimer laser with a wavelength of 248 nm and a XeCl excimer laser with 308 nm are used. The height of the profiles is reduced to about 8 mm with the use of telescopes to direct the full height of the beam onto the beam homogenizers, which reduce spatial fluctuations of the beam profile [21]. Afterwards, the beam has a height of about 20 mm and is slightly diverging. Then, a thin light sheet of about 400 µm thickness in the measurement area is formed with cylindrical plano-convex lenses. The two beams are overlapped using a dichroic mirror and their height is reduced by an aperture so that reflections on the inner surfaces of the cells are avoided. For calibration measurements the height is reduced to 20 mm and for the spray measurement to 50 mm. The reflection on a fused silica glass plate in front of the cell is measured with an energy meter to correct laser intensity fluctuations between measurements. The beam is then directed through the cell or test rig and absorbed totally in a beam dump. Fluorescence is detected perpendicular to the laser light sheet. Elastically scattered light from the lasers is blocked with a 355 nm longpassfilter. The signal is acquired with an ICCD camera with an exposure time of 240 ns to avoid the detection of the longer lasting phosphorescence that occurs for lower oxygen partial pressures [3]. For the calibration measurements an Andor iStar camera is used with a 4 x 4 binning to reduce camera gain and noise, as no spatial resolution is required. For the spray investigation a PCO DiCam with double-shutter mode and no binning is used. The time delay between the two different images is set to 5 µs.

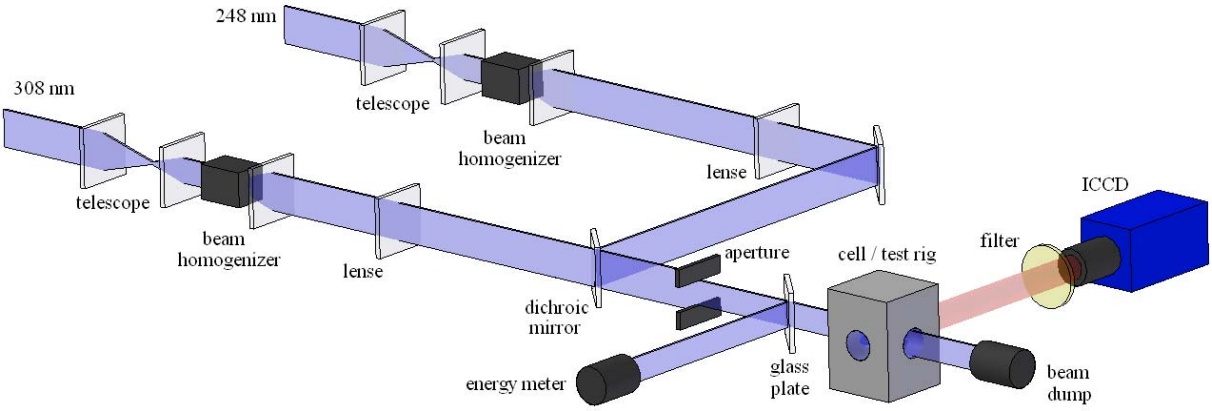

Figure 1: Optical setup for calibration and spray measurement

Tracer calibration

The calibration of the tracer 3-pentanone is carried out at 0.8 MPa and different temperatures up to 673 K in nitrogen atmosphere. A total of 50 single-shot images of 248 nm and 308 nm excitation are acquired and averaged for each calibration point. Additionally, images in pure nitrogen without tracer are recorded to remove background signal from the calibration images in the evaluation process. As the tracer density is know also absorption effects of the laser beam inside the cell can be corrected using the Beer-Lambert law

$$T_\lambda = e^{\left(\frac{\rho}{M} \cdot N_A \cdot l \cdot \sigma(\lambda,T)\right)} \tag{5}$$

where T_λ is the transmission, ρ is the tracer density, M is the molar mass, N_A is the Avogadro constant, l is the path length of the beam and $\sigma(\lambda,T)$ is the absorption cross section depending on temperature T and wavelength λ. The signal ratio for the temperature calibration is built from the averaged and corrected images. The ambient pressure of 0.8 MPa is kept constant during spray measurements and calibration, so the signal intensity S_x of each wavelength x and the signal ratio S_{ratio} can be described by the interpolation functions of the calibration points at 0.8 MPa depending only on temperature T and tracer density ρ. These functions can be inverted to the calibration functions for temperature and density. From the tracer density the mass fraction of the fuel can easily be calculated under known boundary conditions. Due to the higher laser pulse intensity and better beam homogeneity of the KrF laser in the spray measurement the wavelength of 248 nm was chosen to evaluate the density. Additionally, the concentration of the reference image ρ_{ref} is needed. The calibration was carried out up to 673 K, which is thus the limit for the valid use of these calibration functions for 3-pentanone at 0.8 MPa:

$$T = \frac{-49{,}420 + 118{,}039 \cdot S_{ratio}}{1 + 210 \cdot S_{ratio} - 6.16 \cdot S_{ratio}^2} \tag{6}$$

$$\rho = \rho_{ref} \cdot S_{248} \cdot \frac{1 - 0.003 \cdot T + 3.14 \cdot 10^{-6} \cdot T^2}{1.05 - 0.003 \cdot T + 2.2 \cdot 10^{-6} \cdot T^2} \tag{7}$$

The accuracy of the calibration is calculated with error propagation from the influence of the mass flow controllers, pressure transducer, shot noise of the camera, laser intensity measurement and thermocouple. As the influence of the tracer density cancels out for the temperature calibration the error of the tracer mass flow controller is not considered there, which leads to a higher inaccuracy for the averaged temperature of 3.3% compared to 4.9% for the tracer concentration. To include the influence of the error of the function interpolation on the accuracy and estimate the fluctuations in a homogeneous image of the calibration measurement, the single-wavelength images of the calibration are arranged in pairs of different wavelengths and analyzed with the software routine used for the spray measurement evaluation. The 50 result images are evaluated in a region of interest (ROI) of 680 pixels in the center of the image and then averaged. At 663 K and 0.8 MPa in the calibration cell with a reference tracer concentration of 30 g/m^3 the inaccuracy of the averaged temperature is ±8 K with fluctuations in the ROI of ±7 K (1σ standard deviation). For the averaged concentration the inaccuracy is ±1.7 g/m^3 with fluctuations of ±0.6 g/m^3 (1σ standard deviation) inside the ROI. These low fluctuations could be obtained although the images in the calibration measurement are not acquired quasi-simultaneously, which is a proof of a very homogeneous mixture inside the cell.

Simulation model

One major aim of the measurement technique presented in this paper is the improvement and validation of spray models. Therefore, the measurement results are compared to an Euler-Lagrange spray model with a transient RANS (Reynolds Averaged Navier Stokes) approach. The spray model is set up with a mesh volume of 26 x 26 x 100 mm^3 with a mesh resolution of 300 µm and a calculation step size of 2.5 µs with the 3D-CFD-Code OpenFoam 1.5. Only one jet of the 6-hole injector is modeled. The surrounding atmosphere is defined as quiescent at initial conditions. All relevant sub-models for the spray processes atomization (Enhanced Taylor-Analogy-Breakup model [22]), droplet collision (trajectory [23]), turbulent droplet dispersion (stochastic dispersion), evaporation (infinite diffusion model, see e.g. [24]) as well as droplet drag and turbulence (RNG k-epsilon) are included for a realistic spray representation. Details of the principle calibration strategy setup of the model can be found in ref. [16].

Spray experiment preparation

The operating conditions in the test rig are set to 673 K and 0.8 MPa and are kept constant throughout the measurement. Integral Mie scattering measurements under the same conditions show that 2 ms after visual start of injection (vSOI) clearly no liquid phase is left in the jet, only small amounts are detected close to the nozzle probably due to unwanted post-injection (needle bouncing). This has to be assured as the calibration is only valid in the vapor phase and liquid tracer droplets would induce large errors into the measurement. Therefore, the spray is investigated at 2 ms, 2.5 ms and 3 ms after vSOI to get information about the evaporation rate and the entrainment of hot surrounding air into the jet. For each time step 32 double-shutter images of the spray are acquired with a frequency of 0.5 Hz to ensure complete flushing of the measurement area between injections.

The image for background correction is simply recorded without injection but with both lasers running to get the background signal from reflections especially on the injector tip. A reference image with a homogeneous and known tracer density for the quantification of the density in the spray has to be acquired for each excitation wavelength. For the reference images, the inlet and outlet valves of the rig are closed so that it is not scavenged during the measurement and pure 3-pentanone is injected into the chamber at 423 K and 1 MPa to avoid thermal

decomposition [19] or condensation of the tracer. After 180 injections and an additional mixing time of about 1 min a homogeneous and dense enough tracer concentration for a good signal-to-noise ratio (SNR) is achieved. A total of 32 images are recorded and averaged to gain a low-noise reference image. Although the tracer distribution in the field of view is homogeneous during the reference measurement, the exact density is unknown as the diffusion into the insulation ceramics, supply and output connections cannot be quantified. To quantify the reference concentration, the absorption effects in the field of view are calculated using the Beer-Lambert law (Eq. 5). Spatial inhomogeneities of the camera and intensifier are canceled out by building a ratio of the signal of both wavelengths. The remaining decay of the signal ratio along the beam path is the result of the wavelength dependent absorption behavior. By building a transmission ratio using the Beer-Lambert-law and comparing it with the measured signal ratio, a corresponding reference density of 142 g/m^3 is calculated for the measurement. The deviation between the measured and calculated absorption ratio along the beam path is 0.66% (1σ standard deviation).

Results and Discussion

The 32 double-shutter images from the measurement are background corrected and normalized to the reference. By this, also spatial fluctuations of the two laser beams are canceled out. Afterwards, the temperature and tracer density are analyzed by means of the calibration data. With this information the spatial absorption effects in the spray can be calculated using the Beer-Lambert law. The raw images are absorption corrected and analyzed again to obtain the absorption corrected temperature and tracer density. The mass fraction of the fuel (complete iso-octane/3-pentanone mixture) is then calculated from the tracer density. For a comparison with the simulation, which uses a statistical approach (RANS), the 32 single result images are averaged. As the spray itself has cyclic fluctuations and is not in the same spots for each measurement, a temperature of 673 K and a tracer density of 0 g/m^3 are assumed for averaging when no signal is obtained.

Figure 2 shows the averaged results of the temperature (left upper part) and mass fraction of the fuel vapor (left lower part) of the spray at 2.5 ms after vSOI. The positions of the nozzle as well as a radial line at the distance of 40 mm from the nozzle in the right jet are also marked. The temperature is lowest around the axis of the spray and increases away from the axis due to the dilution with the hot surrounding air. This can also be seen in the mass fraction of the fuel, which decreases in radial direction. Close to the nozzle large temperature gradients occur due to liquid fuel residuals of unwanted post-injection as mentioned above. Due to the spray angle, a length of about 60 mm of the jet is homogeneously illuminated by the 50 mm high laser light sheets. Thus, the later given error estimation is only valid up to 60 mm, but the results beyond that point can still be interpreted qualitatively to estimate the penetration depth or shape of the jet.

For further evaluation and a better comparison with the simulation, the temperature (right upper part) and fuel vapor mass fraction (right lower part) profiles along the 40 mm line are also shown in figure 2 together with the corresponding results from the simulation. The results are shown for 2.5 ms and 3 ms after vSOI. At 2.5 ms after vSOI a minimum temperature of 541 K is measured close to the axis of the spray, which corresponds to a cooling of 132 K. With 577 K the minimum temperature of the simulation is 36 K higher than measured. The right side of the jet away from the injector shows a broader profile with a stronger cooling than the simulation. Similar results can be seen for the mass fraction, which is with a maximum value of 0.11 lower in the simulation than in the measurement with 0.15. Also the right side of the jet is broader and has a higher mass fraction. Overall, the vapor mass fraction is higher and therefore the temperature is lower at this time point due to the stronger cooling in the experiment than in the simulation at 40 mm distance from the nozzle and 2.5 ms after vSOI. At 3 ms after vSOI the mass fraction of the fuel decreases and the temperature increases due to the entrainment of hot surrounding air. The minimum measured temperature of 591 K is very close to the simulation result of 601 K. Furthermore, the shape of the temperature profile as well as the vapor jet width for measurement and simulation are almost identical. Still, the mass fraction is underestimated in the simulation with 0.074 compared to the measured 0.11. But again the shape of the profile and the jet width are very similar.

The major differences between the measurement and the simulation can be explained by model inaccuracies especially of the turbulence model. The drift of the spray tail due to spray-induced turbulence is larger in the measurement than in the simulation. Additionally the spray is stretched, which leads to an about 5% larger liquid penetration and longer spray at the end of injection due to simplified sub-models and boundary conditions accounting for atomization and evaporation. Therefore, the local fuel vapor mass fraction in the measurement is larger shortly after the end of injection, which leads to a stronger cooling. At later times the higher spray-induced turbulence in the experiment causes an increased entrainment of the hot surrounding gas, which increases the temperature more rapidly, so that the temperature difference between 2.5 ms and 3 ms is higher in the experiment than in the simulation. The large scale turbulence structures in the vapor are visible in the single-shot results, see figure 3.

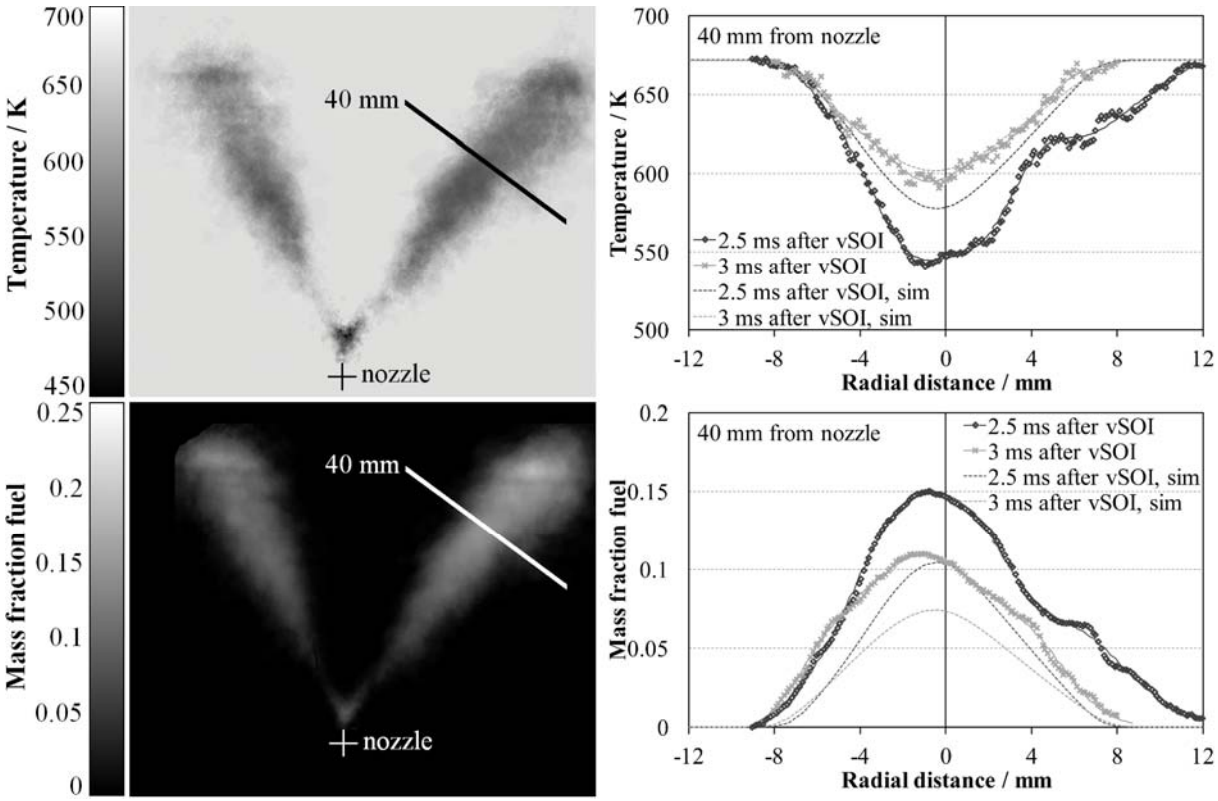

Figure 2: Averaged temperature (left upper part) and mass fraction of the fuel vapor (left lower part) of the spray at 2.5 ms after vSOI; temperature (right upper part) and mass fraction (right lower part) profiles at 2.5 ms and 3 ms after vSOI for ensemble averaged measurement and simulation.

Additionally to the comparison of the experiment with the simulation, those single-shot measurements are analyzed to verify the capability of the measurement technique to resolve cyclic variations. Figure 3 shows the single-shot results of temperature (left upper part) and mass fraction of the fuel vapor (left lower part) of the broadest measured jet at 40 mm distance from the nozzle of the 32 single-shot measurement at 2 ms after vSOI. It can be seen that the structure of the jet can clearly be resolved in the temperature and especially the mass fraction. Compared to averaged results the gradient at the edges of the detected jet is steeper for the single-shot measurement. The reasons for this are shot-to-shot fluctuations of the spray, which result in a smoothening of the edges after averaging. This can also be explained by investigation of different single-shot measurements. Therefore, figure 3 also shows the profiles of temperature (right upper part) and mass fraction of the fuel vapor (right lower part) for four different extreme results as well as the averaged result over all 32 measurements. Shown are the results of the broadest, the narrowest, the farthest right and the farthest left shifted jet at 40 mm distance from the nozzle of all 32 single-shot measurements. Again, the gradients of temperature and mass fraction are steeper at the edges for the single-shot measurements. For further evaluation the axis of the spray is assumed to be in the middle between the left and the right end of the detected vapor phase despite the aerodynamic bending of the spray. The shot-to-shot fluctuations of the axis are then 1.66° (1σ standard deviation) with a maximum deviation of 4.6° for the furthest right and 7.0° for the furthest left jet. It has to be mentioned that the change of the width does not necessarily mean a bent of the spray axis as it could be the result of a local eddy at the distance of 40 mm from the nozzle that broadens the jet there to one side. Thus, the given fluctuation of the axis can be seen as a worst case fluctuation. Additionally to the axis, the width of the jet is also changing from pulse to pulse. The ensemble averaged jet width is 12.6 mm with a fluctuation of 1.9 mm (1σ standard deviation) over the 32 measurements, which corresponds to 15.1%. The narrowest jet has a width of only 9.5 mm and the broadest jet, which is shown in Figure 3 (left), has a width of 16.5 mm. Due to these fluctuations the gradient on the edges of the jet is smoothed by averaging. Despite these large spatial cyclic fluctuations the local minimum and maximum values of temperature and mass fraction in the individual jets are small. For 2 ms after vSOI a maximum cooling to 523 K is visible in the averaged result, similar minimum temperature is detected in the center of all 32 jets. The same can be seen for the mass fraction, where an averaged maximum of 0.21 is measured. Locally the differences might be high, but this is mainly because of the fluctuation of the spray position, the deviations in evaporation rate and cooling are small compared to that.

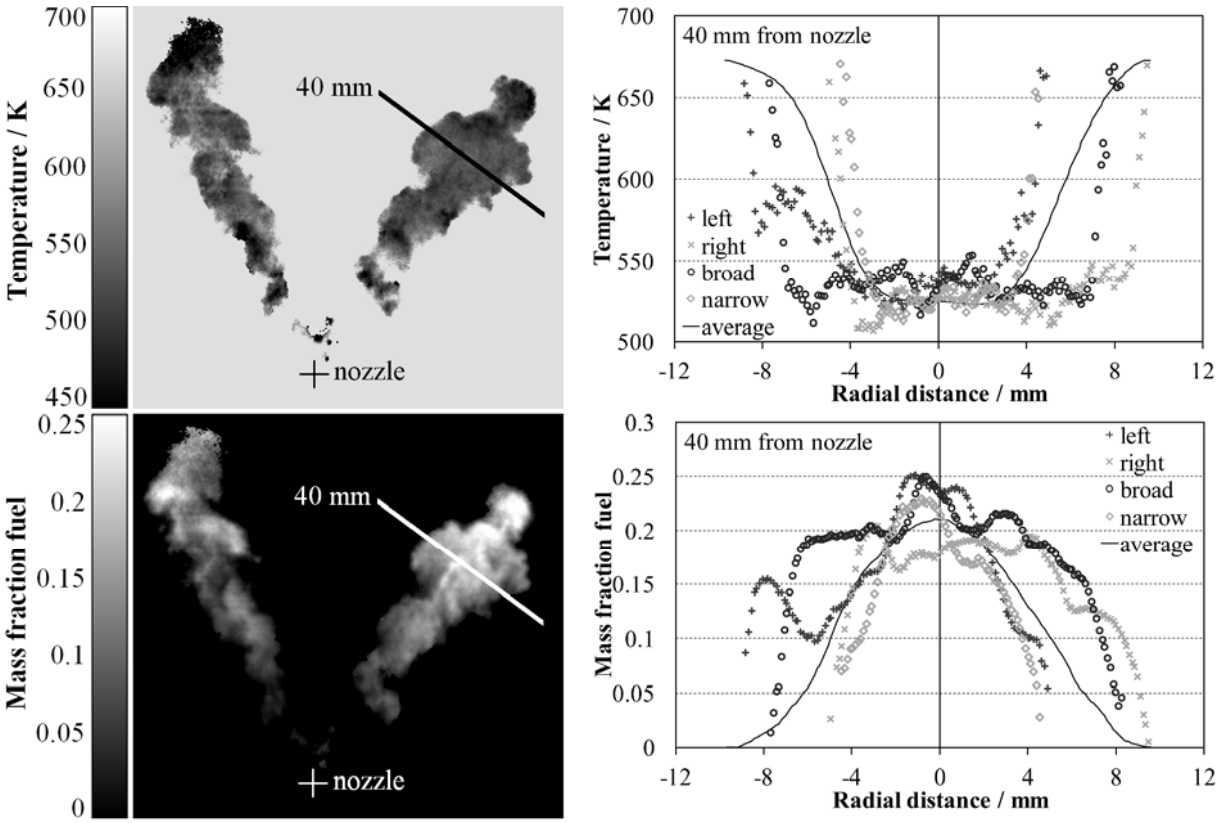

Figure 3: Temperature (left upper part) and mass fraction of the fuel vapor (left lower part) of a single-shot measurement of the spray with the broadest jet at 40 mm distance from the nozzle at 2 ms after vSOI; temperature (right upper part) and mass fraction (right lower part) profiles at 2 ms after vSOI in 40 mm distance from the nozzle for averaged result as well as single-shots of the broadest, narrowest, farthest left and farthest right shifted jet of the 32 single-shot measurements

Error analysis

To validate the presented technique for measurements in the spray for single-shot and averaged results a detailed error analysis is carried out. For the averaged results the accuracy can be calculated with error propagation from the accuracy of the calibration, pressure, temperature field in the chamber and camera linearity, for single-shot measurements additionally the camera noise and laser intensity fluctuations have to be considered. This gives an inaccuracy of 3.8% for temperature and 5.2% for mass fraction for ensemble averaged results. For single-shot measurements an inaccuracy of 5.6% for temperature and 6.6% for mass fraction can be achieved. The accuracy of the temperature is higher because of the higher temperature calibration accuracy as the influence of the tracer concentration cancels out.

An estimation of the precision of the spray measurements is difficult due to the spatial shot-to-shot fluctuations of the jet mentioned above that are much higher than the actual measurement errors. Therefore, the precision is determined with the homogeneous reference images of the spray measurement (1 MPa, 423 K, mass fraction 0.15) as no spatial shot-to-shot fluctuations occur here. The 32 reference images are analyzed with the same routine used for the evaluation of the spray measurement. All deviation values that are given here are 1σ standard deviations. The ensemble averaged reference is evaluated in an ROI of 102,676 pixels in the region of the examined spray jet to obtain a spatial precision within one averaged result image, which is ±2.4 K for the temperature and ±0.0011 for the mass fraction, corresponding to relative standard deviation of 0.6% and 0.8%, respectively.

To determine the single-shot precision, the single-shot reference images are also evaluated separately. They have a shot-to-shot fluctuation of ±15 K (3.6%) for the spatial averaged temperature and ±0.0081 (5.5%) for the spatial averaged mass fraction. The evaluation of the single images in the same ROI as for the ensemble averaged results shows a spatial precision of ±7-10 K (1.7-2.4%) and ±0.0035-0.0054 (2.4-3.7%). However, the measurement is influenced by different injected mass of each injection hole resulting from different nozzle discharge coefficients. Possible additional errors in the spray are difficult to estimate as the spray itself has a strong cyclic fluctuation due to its turbulent nature.

Conclusions

The present paper shows the results of a simultaneous spatial resolved measurement of fuel vapor mass fraction and temperature of an evaporating iso-octane spray under DISI-engine conditions with two-line PLIF and 3-pentanone as tracer. The measurements were conducted in an optically accessible combustion test rig for iso-octane in nitrogen atmosphere at 0.8 MPa and 673 K. The tracer was calibrated in a high temperature calibration cell at these conditions with an inaccuracy of 3.3% for temperature and 4.9% for mass fraction measurements.

Averaged results over 32 measurements were evaluated and compared to a CFD-simulation under the same conditions. Overall, experiment and simulation are in good agreement as the shape and size of the ensemble averaged jet as well as temperature and mass fraction gradients are similar. The measurement shows a slightly shorter spray with stronger cooling and higher mass fractions early after vSOI, which can be explained by model inaccuracies especially of the turbulence model. Evaluation of the single-shot results shows strong cyclic fluctuations of the jet. Deviations of the jet axis of 1.66° and of the jet width of 15.1% are measured at 2 ms after vSOI. The single-shot results also show that the gradients are steeper than for the averaged result, where they are smoothened due to averaging of the spatial spray fluctuations.

A detailed error analysis gives inaccuracy for ensemble averaged measurements in the jet of 3.8% for temperature and 5.2% for mass fraction with a spatial precision of 0.6% and 0.8%, respectively. Single-shot measurements show an inaccuracy of 5.6% for temperature and 6.6% for mass fraction. The spatial precision of the single-shot measurements is 1.7-2.4% for temperature and 2.4-3.7% for mass fraction.

The measurements and simulation clearly show that PLIF is a suitable method to determine temperature and mass fraction of the fuel vapor in an evaporating DISI spray under engine relevant conditions. With this information spray parameters such as evaporation rate can be determined, which allows an analysis of the influence of boundary conditions on the spray behavior as well as an improvement of spray models.

Acknowledgements

The authors gratefully acknowledge the financial support of parts of this work by the German Research Foundation (DFG) which also funds the Erlangen Graduate School in Advanced Optical Technologies (SAOT) within the framework of the German Excellence Initiative.

References

[1] Birkigt, A., Michels, K., Theobald, J., Seeger, T., Gao, Y., Weikl, M. C., Wensing, M. and Leipertz, A., *International Journal of Engine Research* 12:282-292 (2011).
[2] Thurber, M. C. and Hanson, R. K., *Appl. Phys. B* 69:229-240 (1999).
[3] Löffler, M., Beyrau, F. and Leipertz, A., *Appl. Optics* 49:37-49 (2009).
[4] Einecke, S., Schulz, C. and Sick, V., *Appl. Phys. B* 71:717-724 (2000).
[5] Rothamer, D. A., Snyder, J. A., Hanson, R. K. and Steeper, R. R., *Appl. Phys. B* 99:371-384 (2010).
[6] Koban, W., Koch, J. D., Sick, V., Wermuth, N., Hanson, R. K. and Schulz, C., *Proc. Combust. Inst.* 30:1545-1553 (2005).
[7] Luong, M., Zhang , R., Schulz, C. and Sick, V., *Appl. Phys. B* 91:669-675 (2008).
[8] Devillers, R., Bruneaux, G. and Schulz, C., *Appl. Phys. B* 96:735-739 (2009).
[9] Kaiser, S. A. and Long, M. B., *Proc. Combust. Inst.* 30:1555 (2005).
[10] Orain, M., Baranger, P., Rossow, B. and Grisch, F., *Appl. Phys. B* 102:163-172 (2010).
[11] Kühni, M., Morin, C. and Guibert, P., *Appl. Phys. B* 102:659-671 (2011).
[12] Zigan, L., Schmitz, I., Flügel, A., Knorsch, T., Wensing, M. and Leipertz, A., *Energy & Fuels* 24:4341-4350 (2010).
[13] Makino, A. and Law, C. K., *Combust. Flame* 73:331-336 (1988).
[14] Zigan, L., Schmitz, I., Flügel, A., Wensing, M. and Leipertz, A., *Fuel* 90:348-363 (2011).
[15] Egermann, J. and Leipertz, A., *SAE Technical Papers Series* 2000-01-2863 (2000).
[16] Zigan, L., Ammon, M., Schmitz, I., Gupta, A., Wensing, M. and Leipertz, A., *SAE Int. J. Fuels Lubr.* 5:254-264 (2012).
[17] Davy, M., Williams, P., Han, D. and Steeper, R., *Exp. Fluids* 35:92-99 (2003).
[18] Schulz, C. and Sick, V., *Prog. Energy Combust. Sci.* 31:76 - 121 (2005).
[19] Eichmann, S. C., Trost, J., Seeger, T., Zigan, L. and Leipertz, A., *Optics Express* 19:11052-11058 (2011).
[20] Vogel, T., Wensing, M., Leipertz, A., Iannuzzi, S. and Lutz, M., *SAE Technical Papers Series* 2011-01-1928 (2011).
[21] Pfadler, S., Beyrau, F., Löffler, M. and Leipertz, A., *Optics Express* 14:10171-10180 (2006).
[22] Tanner, F. X., *SAE Technical Paper Series* 970050 (1997).
[23] Nordin, N. Complex Chemistry Modeling of Diesel Spray Combustion. PhD-Thesis, Chalmers University of Technology, Göteborg, 2001.
[24] Sirignano, W. A., *Fluid Dynamics and Transport of Droplets and Sprays*, Cambridge University Press, Cambridge, U.K., 1999.